Journal of Quantitative Spectroscopy & Radiative Transfer 254 (2020) 107207

Contents lists available at ScienceDirect

Journal of Quantitative Spectroscopy & Radiative Transfer

journal homepage: www.elsevier.com/locate/jqsrt

Near-field plasmonics of gold nanoparticles in dielectric media

Anil Yuksel[a,*], Michael Cullinan[b], Edward T. Yu[c], Jayathi Murthy[d]

[a] IBM Corporation, 11400 Burnet Road, Austin, TX 78758, USA
[b] Department of Mechanical Engineering, The University of Texas at Austin, Austin, TX 78712, USA
[c] Microelectronics Research Center, Department of Electrical and Computer Engineering, The University of Texas at Austin, Austin, TX 78758, USA
[d] Henry Samueli School of Engineering and Applied Science, University of California, Los Angeles, Los Angeles, California 90095, USA

ARTICLE INFO

Article history:
Received 6 November 2019
Revised 3 July 2020
Accepted 8 July 2020
Available online 9 July 2020

Keywords:
Enhanced plasmonic nanoparticles
Dielectric shell
Nanotechnology

ABSTRACT

Metal nanoparticles have attracted intense attention due to their unique optical and thermal properties for applications such as micro-nano electronics and photonics. Relative orientation, interparticle spacing, and particle size strongly impact the optical behavior of the nanoparticle assemblies. The near-field confinement of electromagnetic fields between closely packed metal nanoparticles, which is enhanced due to their plasmonic behavior, creates high thermal energy densities under visible to near-infrared wavelength laser irradiation. As metal nanoparticles tend to be oxidized or change shape under laser illumination, resulting in non-linear optical and thermal behavior, surrounding each metal nanoparticle with a dielectric shell could be a potential way to mitigate these effects as well as to engineer their plasmonic behavior. In this study, we use numerical simulations to analyze the plasmonic behavior of gold (Au) nanoparticles surrounded with dielectric shell by investigating nanoparticle's various configurations to each other as well as their relative orientation to incoming light source under laser irradiation in dielectric media. Such geometries are of particular interest for applications such as photonic integrated circuits, photonic sintering and nanophotonic cooling.

1. Introduction

Plasmon resonances and electromagnetic scattering by metallic nanoparticles are of intense interest for a broad range of applications in nanotechnology [1,2]. Resonance tunability and near-field effects between metallic nanoparticles can strongly influence the energy transport between the nanoparticles in different media. Such effects are of particular interest in practical applications such as photonic integrated circuits, photonic sintering and nanophotonic cooling [3,4]. Previously, dimers [5–7] and different configurations of clusters [8,9] formed from pure metallic nanoparticles have shown strong plasmonic behaviors, which also depend on particle size, polarization, wavelength and configuration. By controlling the electromagnetic wave propagation in nanoparticle assemblies, very strong electromagnetic fields can be achieved via excitation of surface plasmon resonant (SPR) modes that are influenced by the interactions between nanoparticles and their surrounding medium, as well as between the nanoparticles themselves [10,11]. Surface-enhanced Raman spectroscopy (SERS) enhancements are observed, for example, on metallic nanoparticles and agglomerates [12]. Very high SERS enhancements (~10^6–10^8) were reported for very small interparticle spacing between the nanoparticles [13,14]. However, such closely spaced nanoparticles are not consistently reproducible within agglomerates which makes them less practical applications in nanotechnology. In many circumstances, metal nanoparticles are suspended in a dielectric medium such that nanoparticle size, shape, structure and the dielectric medium properties all influence the optical response under illumination [15,16]. Nanoparticle-light interaction can strongly influence heating and energy transport, which become essential in such applications. For example, light can be highly concentrated between the metal nanoparticles suspended in a dielectric medium which results in enhanced near-field thermal energy transport [17,18]. However, metal nanoparticles tend to have high oxidation and dissipation losses that can degrade plasmon propagation. Moreover, agglomeration of metal nanoparticles creates challenges in designing assemblies. One of the methods to prevent oxidization and agglomeration is surrounding the nanoparticles with a dielectric shell. The type of dielectric shell that surrounds the nanoparticles as well as the dielectric medium are observed to affect SPP propagation, and plasmon resonance shift depending on the surrounding medium's thermo-optical properties [16,19]. Thus, the effect of dielectric shell and the surrounding medium properties under laser illumination become very important for near-field energy transport [20,21].

* Corresponding author.
E-mail address: anil.yuksel@utexas.edu (A. Yuksel).

https://doi.org/10.1016/j.jqsrt.2020.107207
0022-4073/

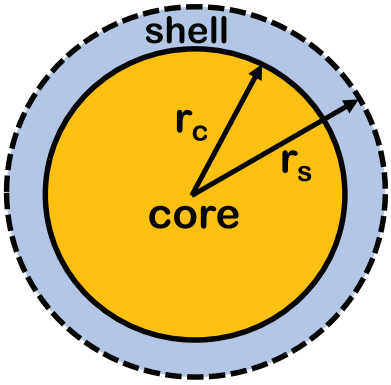

Fig. 1. Spherical nanoparticle with concentric shell.

In this paper, characteristics of optical electromagnetic energy propagation of various size of Au nanoparticle dimers with different relative orientation and 4 nanoparticle chain configurations surrounded by a dielectric shell in different media are determined using finite-difference frequency-domain simulations. Electric field intensity ratio (I/I_0), Poynting vector ratio (S/S_0), extinction cross-section (m^2) are calculated for Au nanoparticles under 400–800 nm and TM polarized laser illumination. The electric field intensity and Poynting vector ratios are defined relative to the incident field intensity (I_0) and incident Poynting vector (S_0), respectively.

2. Modeling analysis

2.1. Theoretical approach

The electromagnetic fields incident on nanoparticles with respect to illuminated laser or light source cause charge oscillations that result in scattering and absorption of electromagnetic radiation. The Mie solution to Maxwell's equations, also known as Lorenz-Mie theory, describes the electric and magnetic fields and electromagnetic scattering by a homogenous sphere. The extension of Mie's theory for a concentric single nanoparticle shell (core-shell) shown in Fig. 1 were investigated by Aden and Kerker [22]. Concentric core-shell structure that each has different material and different thickness (r_c and r_s represents the core and shell radius, respectively) can be characterized with complex refractive index n_c of the core and n_s of the shell. By assuming a nanoparticle is in a non-absorbing medium with real refractive index (n), the wavenumber (k_m) can be expressed as $\frac{2\pi n}{\lambda}$ for plane wave illumination. The scattering and extinction cross-sections of individual nanoparticles are computed based on generalized Lorenz-Mie theory adapted for core-shell particles. The scattering, extinction, and absorption efficiencies are expressed as the following

$$\sigma_{sca} = \frac{2\pi}{k_m{}^2}\sum_{n=1}^{\infty}(2n+1)\left(|a_n|^2+|b_n|^2\right) \tag{1}$$

$$\sigma_{ext} = \frac{2\pi}{k_m{}^2}\sum_{n=1}^{\infty}(2n+1)Re(a_n+b_n) \tag{2}$$

$$\sigma_{abs} = \sigma_{ext} - \sigma_{sca} \tag{3}$$

The coefficients a_n and b_n are

$$a_n = \frac{\psi_n(y)\left[\psi_n{}'(m_2y)+A_n\chi_n{}'(m_2y)\right]-m_2\psi_n{}'(y)[\psi_n(m_2y)+A_n\chi_n(m_2y)]}{\xi_n(y)\left[\psi_n{}'(m_2y)+A_n\chi_n{}'(m_2y)\right]-m_2\xi_n{}'(y)[\psi_n(m_2y)+A_n\chi_n(m_2y)]} \tag{4}$$

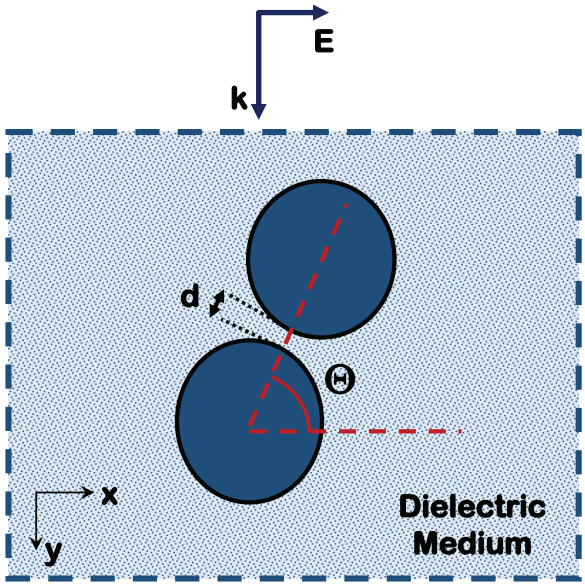

Fig. 2. Modeling geometry: Incident electromagnetic field and nanoparticle dimer suspended in dielectric medium.

$$b_n = \frac{m_2\psi_n(x_r)\left[\psi_n{}'(m_2y)+B_n\chi_n{}'(m_2y)\right]-\psi_n{}'(y)[\psi_n(m_2y)+B_n\chi_n(m_2y)]}{m_2\xi_n(y)\left[\psi_n{}'(m_2y)+B_n\chi_n{}'(m_2y)\right]-\xi_n{}'(x_r)[\psi_n(m_2y)+B_n\chi_n(m_2y)]} \tag{5}$$

$$A_n = \frac{m_1\psi_n{}'(m_2x)\psi_n(m_1x)-m_2\psi_n{}'(m_1x)\psi_n(m_2x)}{m_1\chi_n{}'(m_2x)\psi_n(m_1x)-m_2\chi_n(m_2x)\psi_n{}'(m_1x)}$$

$$B_n = \frac{m_1\psi_n{}'(m_2x)\psi_n(m_1x)-m_2\psi_n{}'(m_2x)\psi_n(m_1x)}{m_1\chi_n(m_2x)\psi_n{}'(m_1x)-m_2\chi_n{}'(m_2x)\psi_n(m_1x)}$$

where $m_1=\frac{n_c}{n}$, $m_2=\frac{n_s}{n}$, $x=\frac{k_m}{r_c}$ and $y=\frac{k_m}{r_s}$. Also, $\psi_n(x)=xj_n(x)$, $\chi_n(x)=x\gamma_n(x)$, and $\xi_n(x)=xh_n(y)$ are Riccati-Bessel, Riccati-Neumann and Ricatti-Henkel functions, respectively. The prime symbol (') also represents the derivation respect to argument.

2.2. Modeling approach for relative orientation between the dimers

It is observed from our previous studies that metallic nanoparticles suspended in dielectric media typically agglomerate [23] at the nanoscale and the close-packed nanoparticle clusters under laser irradiation result in non-local heat transport and hot spots between particles of different size in cluster groups [24–26]. However, the dependence of the electric field enhancement, which affects the thermal energy transport, on relative orientation of the nanoparticles with different nanoparticle size suspended in various media at the agglomerated condition under laser irradiation hasn't been understood clearly.

In applications such as photonic sintering, nanoparticles are typically deposited in a colloidal solution and can create different cluster forms within such solutions. The analysis of relative angle between a nanoparticle pair and incident laser irradiation, as shown in Fig. 2, is important for further understanding larger-scale nanoparticle cluster modeling results [26,27]. Also, the dielectric medium could potentially change the modes between the particles; hence, investigation of the dielectric medium properties with Au nanoparticles are the motivations for modeling these configurations.

The simulated laser-nanoparticle dimer geometry is illustrated in Fig. 2. In this section, 25 nm, 50 nm and 100 nm radius Au

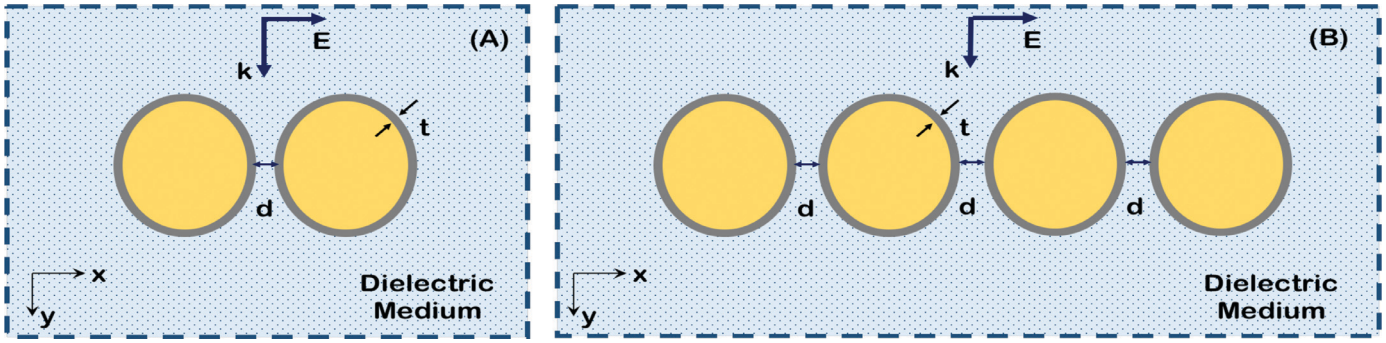

Fig. 3. Modeled geometry for electromagnetic energy and nanoparticle interaction: (A) Nanoparticle dimer suspended in dielectric medium (B) 4 nanoparticle chain configuration suspended in dielectric medium.

nanoparticle dimers which are at different relative orientation with respect to incident laser illumination and suspended in various dielectric media are studied. Three different nanoparticle dimer configurations in which the relative angle (Θ) between the two adjacent nanoparticles and the incident electric field is chosen to be 0°, 30°, 45° and 75° are investigated. The distance between the particles (d) is taken as 1 nm at any analyzed relative orientation for the representation of the typical agglomerated dimer case. In this paper, we use 3-dimensional (3D) finite difference frequency domain method to obtain the electromagnetic field distribution around the metallic nanoparticles by solving Maxwell's equations. The resonant frequency for 50 nm radius gold nanoparticles in water (n=1.33) is approximately 532 nm, which is also a preferred wavelength [28,29]. Thus, we aimed to analyze various nanoparticle size and relative orientation between the dimers under the same wavelength and the dielectric media initially. Thus, pure Au nanoparticle dimers (without dielectric shell) suspended in dielectric medium (n=1.33) are investigated initially under 532 nm and TM polarized light (x direction) as illustrated in Fig. 2 in this section. The complex permittivities of the Au nanoparticles are obtained from Rakic et al. [30]. For the investigated gold nanoparticle size range in this study, the dielectric properties as a function of size is found to be unimportant [31].

2.3. Modeling geometry of dielectric shells in dielectric medium

As agglomeration leads to nanoparticle clustering, electromagnetic wave propagation in such clusters needs to be analyzed. However, the details of electric field enhancement and Poynting vector configurations, which affect the thermal energy transport eventually due to different configuration of nanoparticles surrounded with dielectric shell and suspended into a different dielectric media under laser irradiation wave vector and polarization, haven't been studied in detail.

The orientation of laser irradiation and different simulated core-shell nanoparticle geometries are illustrated in Fig. 3. The shell thickness and the nanoparticle interparticle distance are represented as t and d, respectively. In this section, 50 nm radius Au nanoparticle dimer and 4 particle chain configuration with polyvinylpyrrolidone (PVP) dielectric shell (t=2 nm) and d=1 nm are suspended in various dielectric media. The dielectric properties of PVP are also provided in Fig. 4 [32]. TM polarized (x direction) plane waves propagating in y direction at 400–800 nm wavelength with E_0=1 V/m are investigated. Symmetric boundary conditions are applied due to symmetry between the background field and the particle configurations. Thus, perfect magnetic conductor (PMC) is used at xy symmetry plane for the simulated nanoparticle geometries.

In photonics applications, nanoparticles are generally deposited in aqueous media and nanoparticles could create various configurations within such mixtures. Also, the effect of a dielectric shell that surrounds each Au nanoparticle and the type of dielectric medium in which Au nanoparticles are suspended could potentially exhibit different plasmonic modes between the nanoparticles within such media. Metallic nanoparticles exhibit different plasmonic effects for different configurations when packed closely, and plasmonic behavior will be strongly influenced by a dielectric shell that surrounds each Au nanoparticle and by suspension in different dielectric media (k=0 assumed for all analyzed media), motivating our modeling of the configurations specified in this study. Also, the real (n) parts of the complex refractive index of typical dielectric media typically range between 1 and 1.5. Values of n up to 2 are investigated in this work to illustrate the importance of n on near-field coupling between the Au nanoparticles. This could also provide insight on designing novel solvents.

In this study, the absorption cross-section is obtained by calculating the volume integral of the absorbed energy within the particles. Moreover, by taking the integration of the Poynting vector field over the surface that surrounds the particles at the far-field, scattering cross-section is obtained. Extinction cross-section is determined by sum of scattering and absorption cross-section.

3. Results and discussion

3.1. Effect of particle size and relative orientation on near-field intensity

In simulations of nanoparticle dimers, shown in Fig. 5, the maximum electric field intensity is observed to be as high as 1850 between the 25 nm radius gold nanoparticles and this decreases to 522 and 127 with increasing nanoparticle radius to 50 nm and 100 nm, respectively in a dielectric medium with n=1.33. Higher order interaction modes start to become important with increasing particle size. This leads to reduction of the strength of the dipole-dipole plasmonic modes. Thus, the maximum electric field intensity between the nanoparticles is observed to decrease exponentially with increasing particle size. This exponential decay has been fitted and ~3750exp(−0.035r) where r is the radius of the nanoparticle in dielectric medium (n=1.33) for the investigated three particle sizes is obtained, which is also consistent with Jain et al.'s results [33]. This decrease also implies the reduction of the dipolar plasmon coupling or longitudinal bonding dipole mode (LBDP) strength.

Interparticle dipole-dipole interactions are affected by particle size, relative orientation to the illuminated light source and the suspended dielectric medium characteristics, and electric field enhancement is observed as greater to be for smaller particles with interparticle distance of 1 nm. However, for larger interparticle distance, the maximum electric field enhancement could be observed to depend non-linearly on particle size at off-resonant

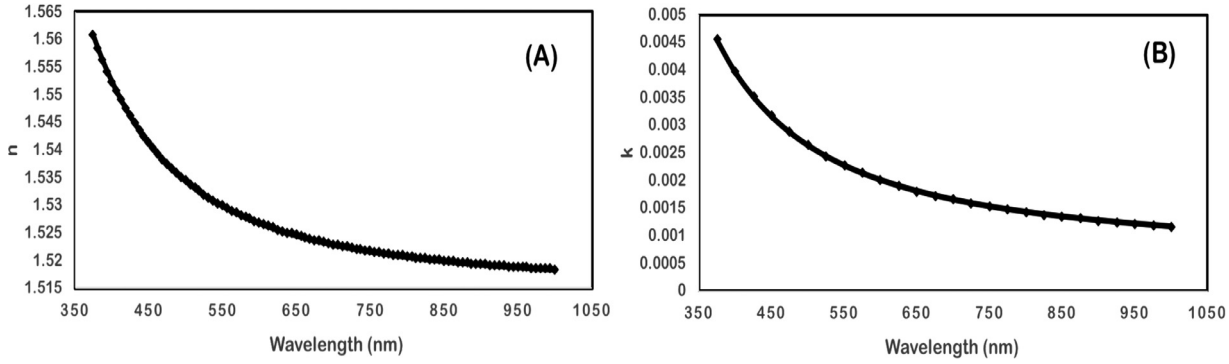

Fig. 4. Dielectric properties of PVP as functions of wavelength: (A) Real (n) and (B) Imaginary (k) parts of the complex refractive index.

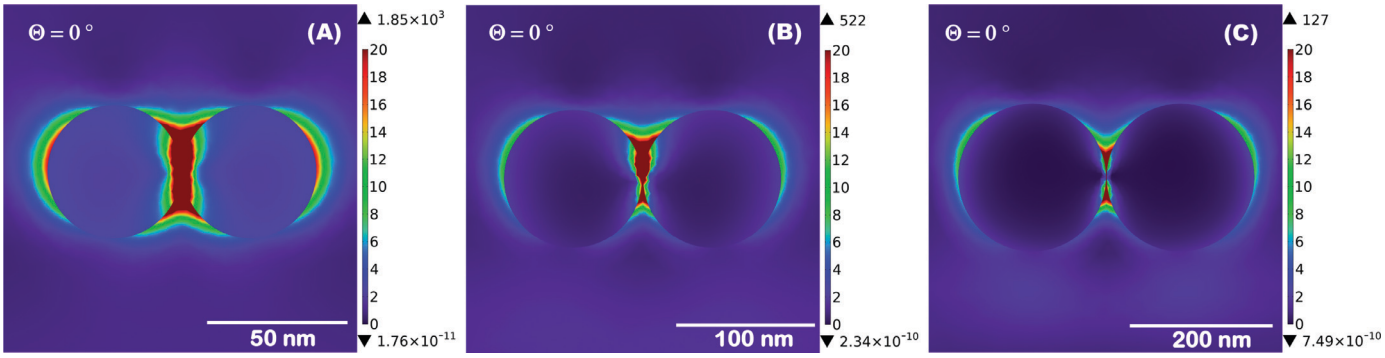

Fig. 5. Electric field intensity ($|I/I_0|$) distribution for Au nanoparticle dimer suspended in dielectric medium (n=1.33) under λ=532 nm, TM polarized light for relative angle (Θ=0°) to electric field: (A) 25 nm radius (B) 50 nm radius (C) 100 nm radius.

Table 1
Calculated Absorption, Scattering and Extinction Cross-section of Au nanoparticle dimer suspended in n=1.33 dielectric medium under 532 nm, TM polarized light.

Radius (nm)	Θ (°)	Absorption Cross-section (x10^4 nm^2)	Scattering Cross-section (x10^4 nm^2)	Extinction Cross-section (x10^4 nm^2)	Extinction Efficiency
25	0	1.24	0.20	1.44	3.67
25	30	1.25	0.21	1.46	3.72
25	45	1.29	0.22	1.51	3.85
25	75	1.40	0.26	1.66	4.23
50	0	3.39	2.49	5.88	3.74
50	30	3.73	2.66	6.38	4.06
50	45	4.44	3.05	7.49	4.77
50	75	5.42	3.43	8.85	5.63
100	0	12.0	16.8	28.8	4.58
100	30	11.5	16.7	28.2	4.50
100	45	10.6	16.5	27.1	4.31
100	75	10.9	15.6	26.5	4.22

wavelength [10]. In fact, plasmon hybridization [34] describes the plasmonic coupling between the nanoparticles with interparticle separation distance. As we aimed to stay in the classical regime in this work, 1 nm is used as a fixed interparticle separation between the nanoparticles in order to prevent the quantum and electron tunneling effects beyond cross-over regime (d < 1 nm) [35,36].

To further understand the plasmon hybridization effect and the higher order mode such as quadruple contributions between closely spaced Au nanoparticle dimers, Θ= 30°, 45° and 75° with varying radius of Au nanoparticle dimer suspended in dielectric medium (n=1.33) are performed. It is observed from Fig. 6 that the maximum electric field intensity is as high as 1480 when the relative angle between the particles and the electric field is 30° for 25 nm radius in the overall studied cases. This decreases to 1180 and 392 with further particle size increase of 50 nm and 100 nm, respectively. However, when increasing θ from 45° to 75° for 100 nm radius of gold nanoparticle dimer, the maximum electric field intensity changes very little. This implies that reduction of near-field enhancement due to dipole-dipole modes is less significant for 100 nm radius gold nanoparticle dimers. This makes sense because the field polarization is almost perpendicular to the gap axis where the contact area gets very narrow so localized surface plasmons are not excited as strongly. We also observe from Fig. 6 that the region within the gap for which very high ($|I/I_0|$>20) field intensity occurs shrinks as the particle radius increases from 50 nm to 100 nm. In particular, plasmonic modes can be defined as bonding, non-bonding, or antibonding based on the plasmon hybridization model [34,37]. As mentioned earlier, the bonding dipole mode are observed at 30°, 45° and 75° for smaller nanoparticle pairs (i.e. 25 nm and 50 nm). Asymmetric bonding modes start to be observed at 50 nm radius gold nanoparticle at higher relative angle (i.e. 75°). Asymmetric bonding quadrupole mode is observed for large nanoparticle radius (i.e. 100 nm) at relative angle higher than 45° [36]. Thus, for nanoparticle radius of 25 nm and 50 nm, Θ is observed to be very important for plasmonic coupling between the nanoparticles suspended in dielectric medium (n=1.33) under λ=532 nm, TM polarized light (x polarized).

Table 1 summarizes the calculated absorption, scattering, and extinction cross-section values for the investigated relative angle and nanoparticle size cases. It is observed that the absorption, scat-

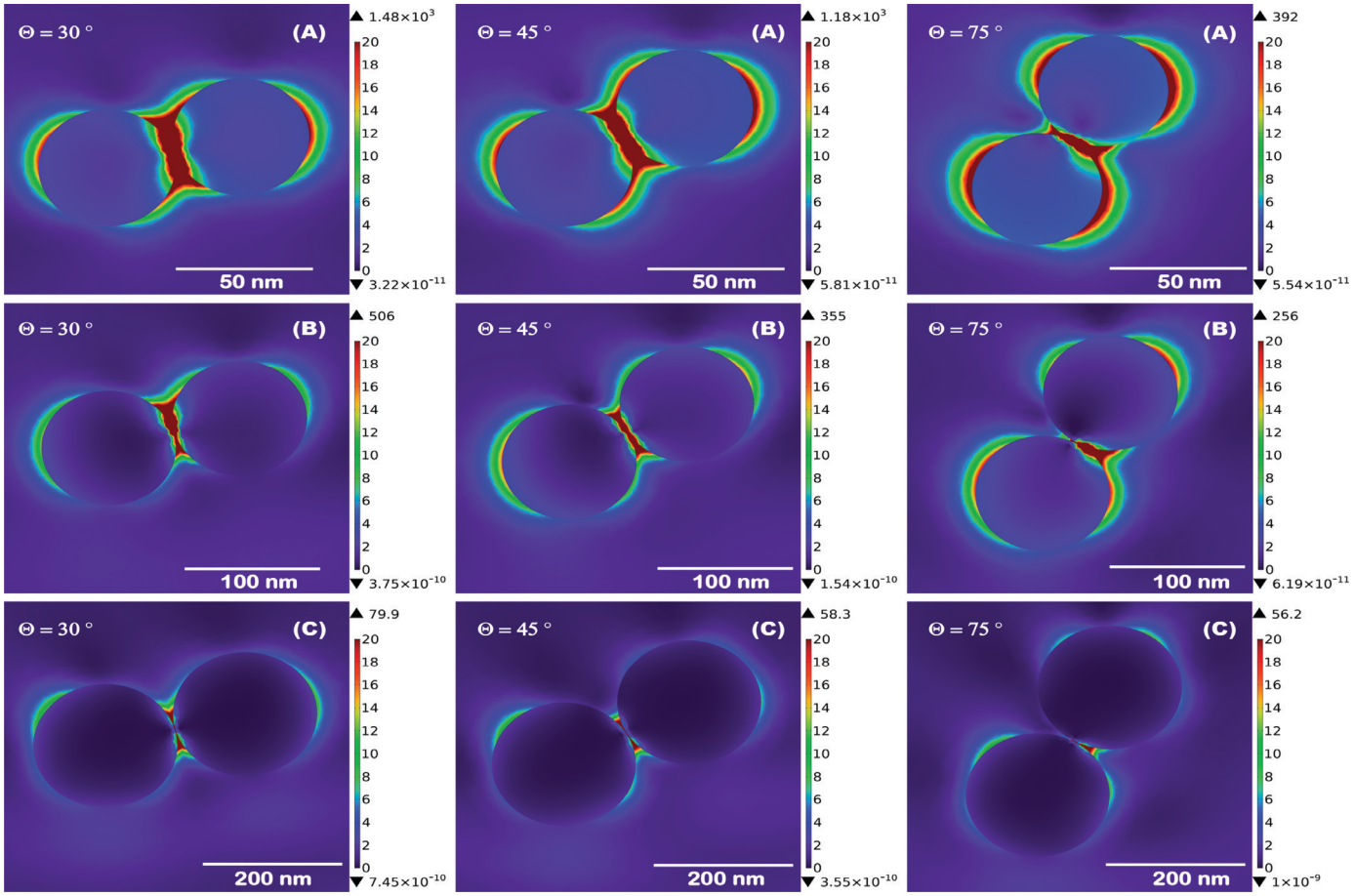

Fig. 6. Electric field intensity ($|I/I_0|$) distribution for Au nanoparticle dimer suspended in dielectric medium (n=1.33) under λ=532 nm, TM polarized light for various different relative angle (Θ) to electric field: (A) 25 nm radius (B) 50 nm radius (C) 100 nm radius.

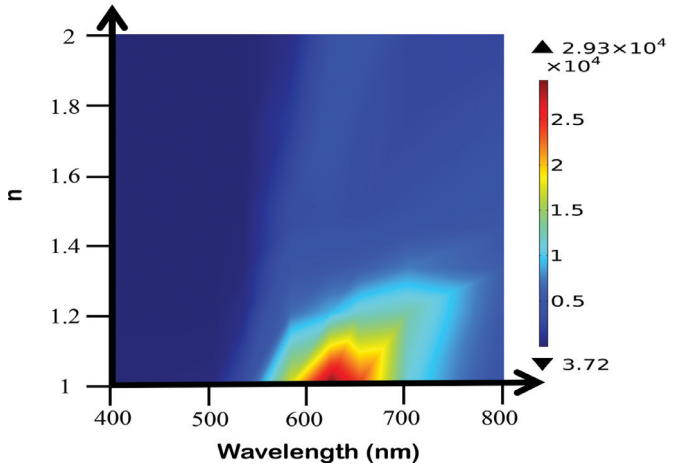

Fig. 7. Maximum electric field intensity ($|I/I_0|$) distribution for 50 nm radius Au nanoparticle dimer suspended in dielectric medium with n ranging from 1 to 2 under λ=400–800 nm, TM polarized laser.

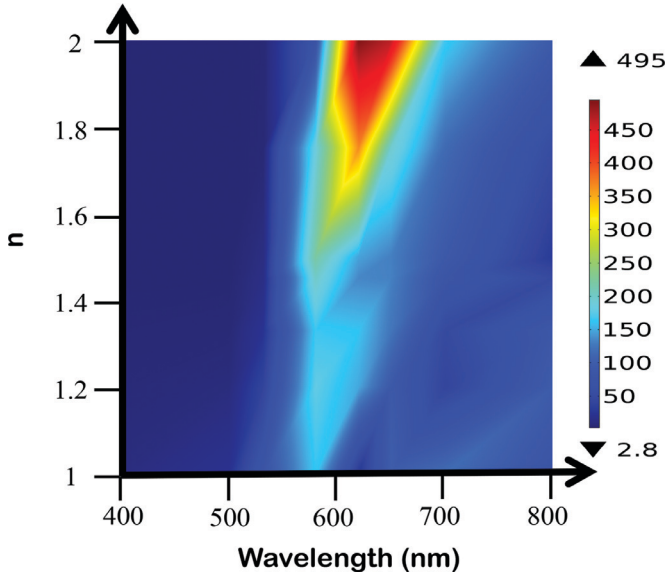

Fig. 8. Maximum Poynting vector ratio (S/S_0) for 50 nm radius Au nanoparticle dimer suspended into various dielectric medium under 400–800 nm wavelength, TM polarized laser illumination.

tering, and extinction cross-sections increase with increasing Θ for 25 nm and 50 nm radius nanoparticle dimers, with this increase being more pronounced for 50 nm nanoparticle radius. This implies that contribution of plasmonic mode is different for different particle size in dielectric medium (n=1.33). As expected, absorption cross-section is dominant over scattering cross-section for 25 and 50 nm radius nanoparticle dimer cases; similarly, scattering cross-section becomes dominant over absorption cross-section for 100 nm radius nanoparticle dimer. Extinction cross-section is also observed to be decreasing for 100 nm radius nanoparticle dimer

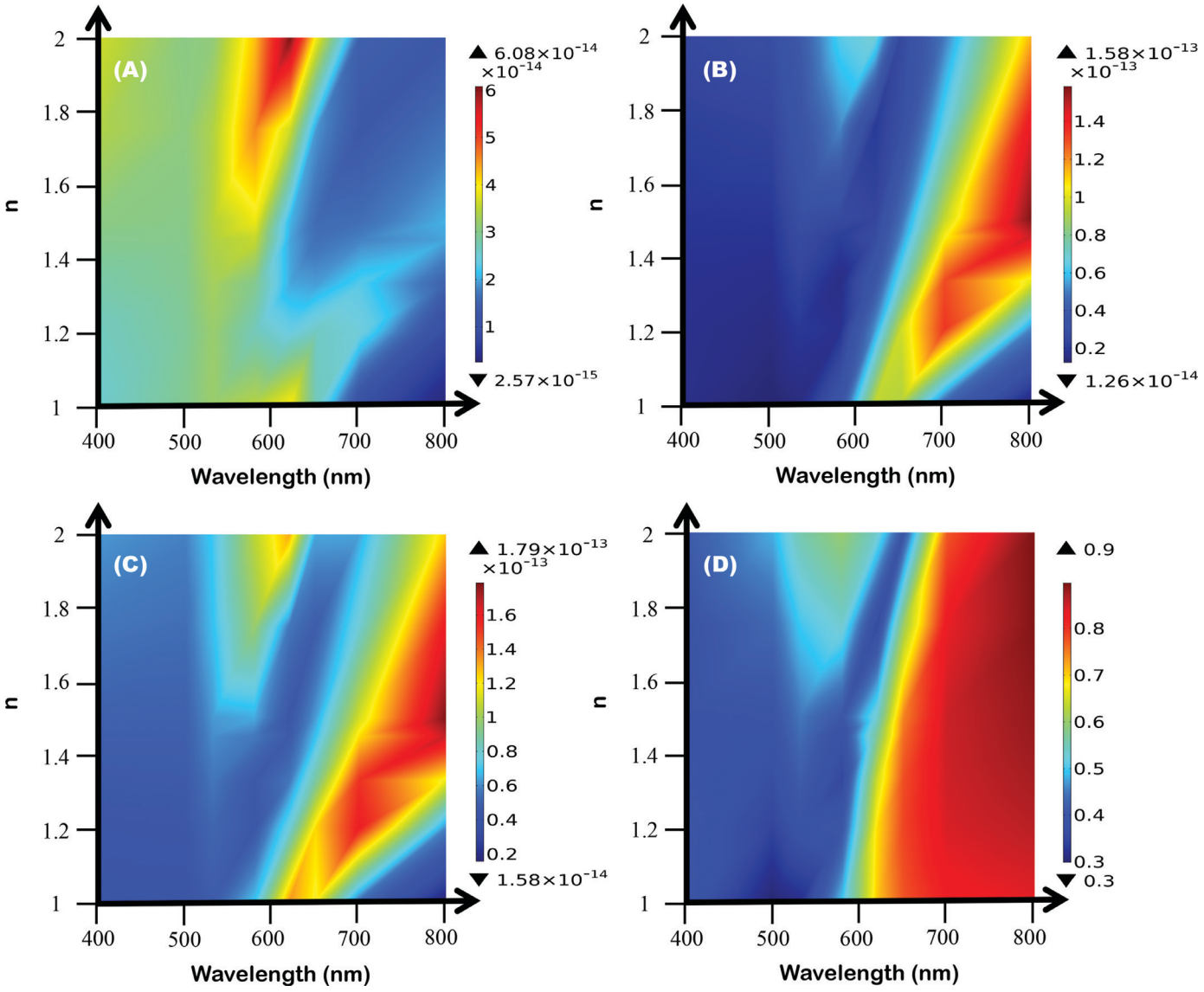

Fig. 9. 50 nm radius Au nanoparticle dimer suspended in various dielectric media of refractive index n under λ=400–800 nm, TM polarized laser: (A) Absorption cross-section (m^2) (B) Scattering cross-section (m^2) (C) Extinction cross-section (m^2) (D) Single scatter albedo (w).

case by increasing Θ. The highest extinction efficiency is observed for 50 nm radius and Θ=75°, which implies that this case is near the plasmon resonance condition in dielectric medium (n=1.33) under λ=532 nm, TM polarized light (x polarized) in overall analyzed various particle size and relative angle cases. This also shows that the maximum electric field intensity for the nanoparticle dimer suspended in dielectric medium doesn't represent the plasmon resonant condition.

3.2. Effect of dielectric shell and dielectric medium on Au nanoparticle dimer configuration

Fig. 7 shows the maximum electric field intensity (I/I_0) under 400–800 nm wavelength, TM polarized laser illumination with 50 nm radius Au nanoparticles with 2 nm thick PVP dielectric shell in the dimer configuration (Θ=0°) suspended in various lossless dielectric media in which n represents the real refractive index of the medium. We observe that the maximum electric field intensity ratio is close to 3×10^4 when the incident wavelength is 620 nm and the Au nanoparticle dimers suspended in n=1 dielectric medium. For n=1, the maximum field intensity decreases with increasing or decreasing the wavelength of the incident laser source, as expected based on the known characteristics of Au nanoparticle plasmonic dipole-dipole gap modes.

Fig. 8 illustrates the maximum Poynting vector ratio (S/S_0) under 400–800 nm wavelength, TM polarized laser illumination with 50 nm radius Au nanoparticles in the dimer configuration suspended in various dielectric media. The maximum Poynting vector ratio is approximately 500 when the incident wavelength is 620 nm and the Au nanoparticle dimers are suspended in n=2 dielectric medium. It is observed that the same 620 nm wavelength results in both the maximum electric field intensity and the maximum Poynting vector ratio; however, in different dielectric media. This could imply that 620 nm is one of the resonant plasmon frequencies for the 50 nm Au nanoparticle dimer (Θ=0°) with 2 nm thick PVP dielectric shell. As enhanced localized plasmon coupling at 620 nm is observed for different dielectric media, near-field plasmonic coupling between the 50 nm Au nanoparticle dimer with dielectric shell is expected to exhibit different optical properties and radiative effects in these dielectric media. To understand such effects in detail, extinction cross-section and single-scatter albedo (w) is calculated for 50 nm radius Au nanoparticle

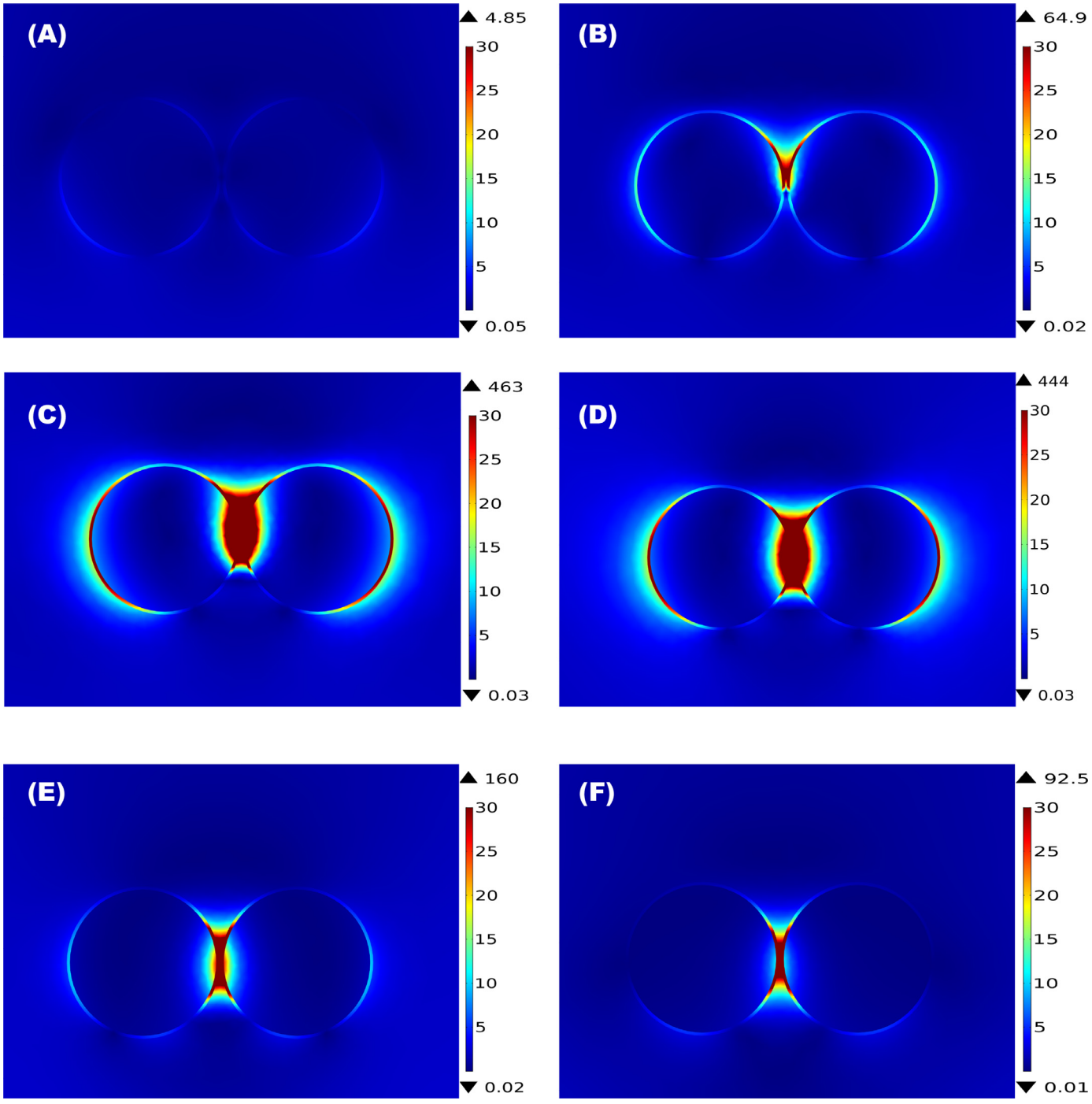

Fig. 10. Poynting vector ratio (S/S_0) at symmetry plane ($z = 0$) for 50 nm radius Au nanoparticle dimer suspended into n=2 dielectric medium under TM polarized laser: (A) λ=532 nm (B) λ=580 nm (C) λ=620 nm (D) λ=650 nm (E) λ=700 nm (F) λ=800 nm.

dimer (Θ=0°) with 2 nm thick PVP dielectric shell suspended in various dielectric media of refractive index n under 400–800 nm wavelength, TM polarized laser as shown in Fig. 9.

Fig. 9(A) shows the absorption cross-section (m^2) for 50 nm radius Au nanoparticle dimer suspended in various dielectric media under 400–800 nm wavelength, TM polarized laser illumination. The highest absorption cross-section is observed at around 620 nm incident wavelength and in n=2 dielectric medium. This implies strong near-field coupling and generation of hot spots between the nanoparticles at 620 nm incident wavelength and n=2 dielectric medium. This is most likely due to the confined dipole-dipole plasmonic modes between the Au nanoparticles in the dimer, for which localized plasmon coupling and interparticle dipole-dipole interaction play a key role to achieve such high absorption cross-section [34,38]. Moreover, decreasing or increasing the wavelength at the same refractive index, n=2 results in reduction of the absorption cross-section. Another observation is that maximum Poynting vector ratio (S/S_0) predicts the wavelength and dielectric medium ranges that give the maximum absorption cross-section, as opposed to maximum electric field intensity ($|I/I_0|$). This

could be because the Poynting vector, which represents the energy flux density of the electromagnetic wave and the photon energy dissipation, provides the right approach rather than the electric field intensity when the absorption cross-section is of primary interest. This observation is corroborated by previously reported results [39].

Fig. 9(C) illustrates the extinction cross-section. It is observed that the 800 nm laser source provides the highest extinction cross-section which is approximately 1.8×10^{-13} m^2, or extinction efficiency of 11.5 when Au nanoparticle dimer is suspended into n=1.52 dielectric medium. This is due to the strong coupling of the quadrupole modes that are observed at such longer wavelengths. At wavelength of 620 nm and n=1.52–2 range, a local peak is observed which is most likely due to dipole-dipole plasmonic mode contribution. So, there are two local peaks (one smaller peak at lower wavelength and one larger peak at higher wavelength) in Au nanoparticle dimer's extinction spectrum when suspended in n=1.52–2 dielectric media. This is due to highly non-linear plasmon hybridization between the nanoparticle dimer in dielectric media [40,41]. It is also observed that 50 nm Au nanoparticle dimer (Θ=0°) with 2 nm thick PVP dielectric shell under 800 nm, TM polarized light and suspended in n=1.52 has extinction efficiency approximately two times higher than that of the pure 50 nm Au nanoparticle dimer (Θ=75°) under 532 nm, TM polarized light and suspended in n=1.33 medium (most preferred case in the literature by researchers) shown in Table 1. Thus, near-field coupling via plasmonic gap modes between particles with dielectric shells occurs under different conditions than for pure nanoparticle dimers.

Fig. 9(D) shows the single-scatter albedo (w) which is the ratio of scattering cross-section to extinction cross-section. It is observed that scattering cross-section is dominant over absorption cross-section by about nine times at wavelength between 720 nm and 800 nm regardless of the dielectric medium, n, which is between 1 and 2. Thus, extinction cross-section is mainly contributed by scattering cross-section at these wavelengths. However, absorption cross-section is dominant over scattering cross-section by about seven times when 50 nm Au nanoparticle dimer (Θ=0°) suspended in dielectric medium, n, between 1 and 1.33 and under the illuminated wavelength between 400 nm and 550 nm. Another observation is that absorption cross-section is dominant over scattering cross-section by about three to four times higher regardless of the analyzed dielectric media between 400 and 500 nm wavelength. Scattering and absorption cross-section are pretty much observed as not a function of dielectric media between 400 and 500 nm wavelength range.

Fig. 10 illustrates the maximum Poynting vector ratio (S/S_0) for 50 nm radius Au nanoparticle dimer suspended into n=2 dielectric medium under TM polarized laser at different wavelengths. It is observed that the Poynting vector ratio (S/S_0) is strongest for a relatively narrow range (~30 nm) of wavelengths (~620 nm) which presumably corresponds to the associated plasmonic dipole-dipole mode. It is also observed that the maximum Poynting vector ratio (S/S_0) is not observed at symmetry plane ($z = 0$) but instead occurs closer to around $z = 1$ nm towards in plane direction which is perpendicular to the illumination and field polarization. It can be seen from Fig. 10(C) which illustrates the strong near-field coupling at 620 nm. This is due to the localized plasmon coupling that generates such hot spots which eventually result in enhanced thermal transport between the nanoparticles. Energy transport as well as the temperature distribution around the nanoparticles are driven by this enhanced localized plasmon coupling due to high electric and magnetic field distribution around and between the nanoparticles. This is associated with hotspots that determine the non-local and non-uniform temperature distribution.

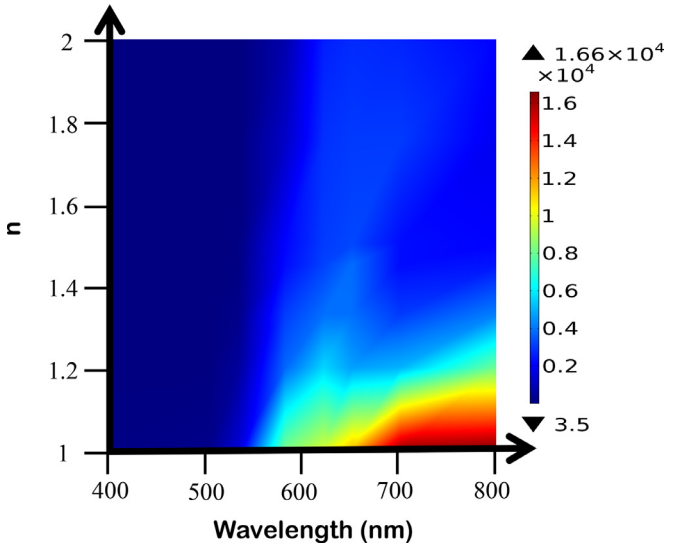

Fig. 11. Maximum electric field intensity ($|I/I_0|$) distribution for 4 particle configuration (chain) of 50 nm radius Au nanoparticle suspended into various dielectric medium under λ=400–800 nm, TM polarized laser.

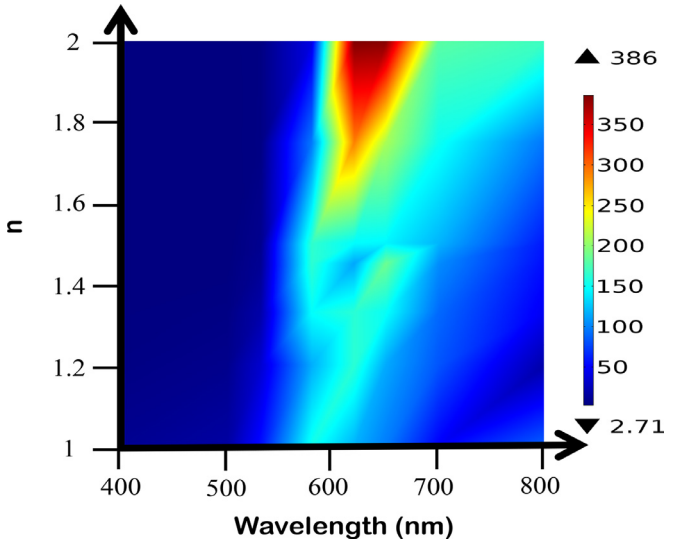

Fig. 12. Maximum Poynting vector ratio (S/S_0) for 4 particle configuration (chain) of 50 nm radius Au nanoparticle suspended into various dielectric medium under λ=400–800 nm, TM polarized laser.

3.3. Effect of dielectric shell and dielectric medium on Au nanoparticle 4 particle chain configuration

Fig. 11 shows the maximum electric field intensity (I/I_0) under 400–800 nm wavelength TM laser illumination with 50 nm radius Au nanoparticles in the 4 particle configuration (chain) suspended in various lossless dielectric media in which n represents the real refractive index of the medium. We observed that the maximum electric field intensity is as high as 1.6×10^4 when the incident wavelength is around 800 nm and the nanoparticles suspended in n=1 dielectric medium. This is about 45% less compared to Au nanoparticle dimer case. It implies that the near-field confinement between the adjacent two nanoparticles in 50 nm Au nanoparticle dimer suspended in dielectric medium with n between 1 and 2 can achieve much higher maximum electric field intensity within 400–800 nm wavelength range than 4 particle configuration (chain). Also, the wavelength dependency for achieving this maximum electric field intensity has broader wavelength

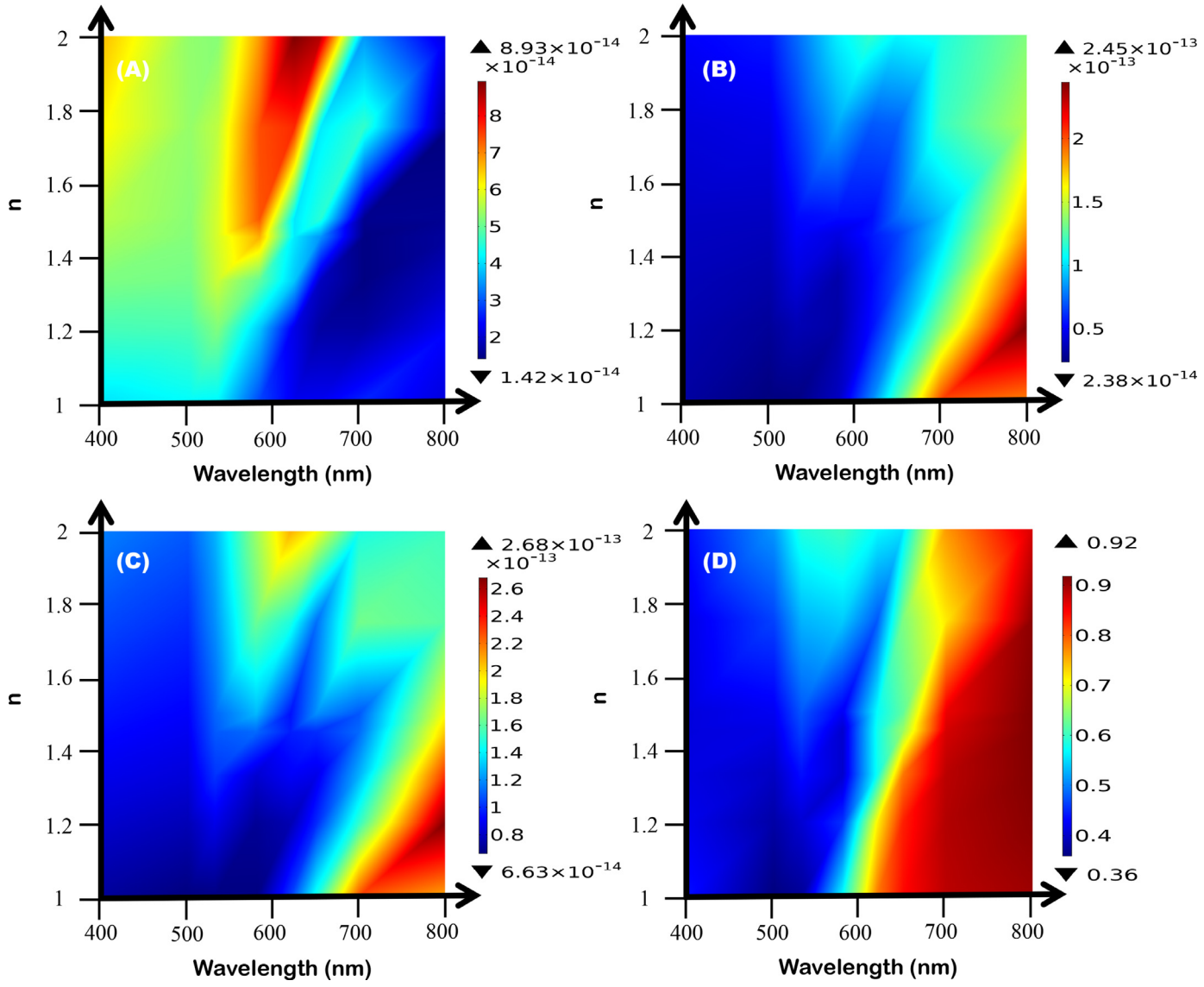

Fig. 13. 4 particle configuration (chain) of 50 nm radius Au nanoparticle suspended into various dielectric medium under λ=400–800 nm, TM polarized laser: (A) Absorption cross-section (m^2) (B) Scattering cross-section (m^2) (C) Extinction cross-section (m^2) (D) Single scattering albedo (w).

spectrum width by about ~100 nm (so the maximum electric field can be achieved approximately within 700–800 nm) than Au nanoparticle dimer case. This decreases with decreasing the wavelength of the incident laser source or increase of the real refractive index of the dielectric medium. This is associated with the collective plasmon modes across multiple particles which characterizes the resonance spectrum. Thus, the maximum electric field intensity shifts towards longer wavelengths at the same dielectric medium (n=1) due to the contribution of the collective plasmon modes. The maximum electric field could locally be much higher but this also doesn't imply the average electric field intensity could also trend in the same way. This also shows that closely spaced 4 particle configuration (chain) suspended in a dielectric medium of 1 leads to shifting the maximum electric field towards higher wavelength within the investigated wavelength range, 400–800 nm.

Fig. 12 illustrates the maximum Poynting vector ratio (S/S_0) under 400–800 nm and TM laser source with 50 nm radius of Au nanoparticle in 4 particle configuration (chain) suspended in various dielectric media. It is observed that the maximum Poynting vector ratio is close to 400 when the incident wavelength is between 620 nm-660 nm and the Au nanoparticles suspended in n=2 dielectric medium, which is about 20–25% lower than nanoparticle dimer case. Similarly, the maximum Poynting vector ratio chain structure has a broader wavelength dependency for the chain structure than nanoparticle dimer case.

The wavelength dependence which is different from Au dimer is due to the near-field plasmon enhancement within many particles that are different from the dimer case. In other words, the effect of additional particles which are closely spaced is to change the interaction between the particles such that the longitudinally aligned dipoles for two adjacent particles give rise to an excitation [42,43]. This coupled collective plasmon-polariton modes in the nanoparticle chain results in interference which is also particle size dependent [44–46]. Thus, the near-field collective resonance for 4 particle configuration has a broader resonant response.

Fig. 13(A) shows the absorption cross-section (m^2) for 50 nm radius Au nanoparticle configuration (chain) suspended into various dielectric medium under λ=400–800 nm, TM polarized laser. It is observed that the highest absorption cross-section is observed at around 650 nm incident wavelength and in n=2 dielectric medium. This implies strong near-field coupling and generation of hot spots at 650 nm incident wavelength and n=2

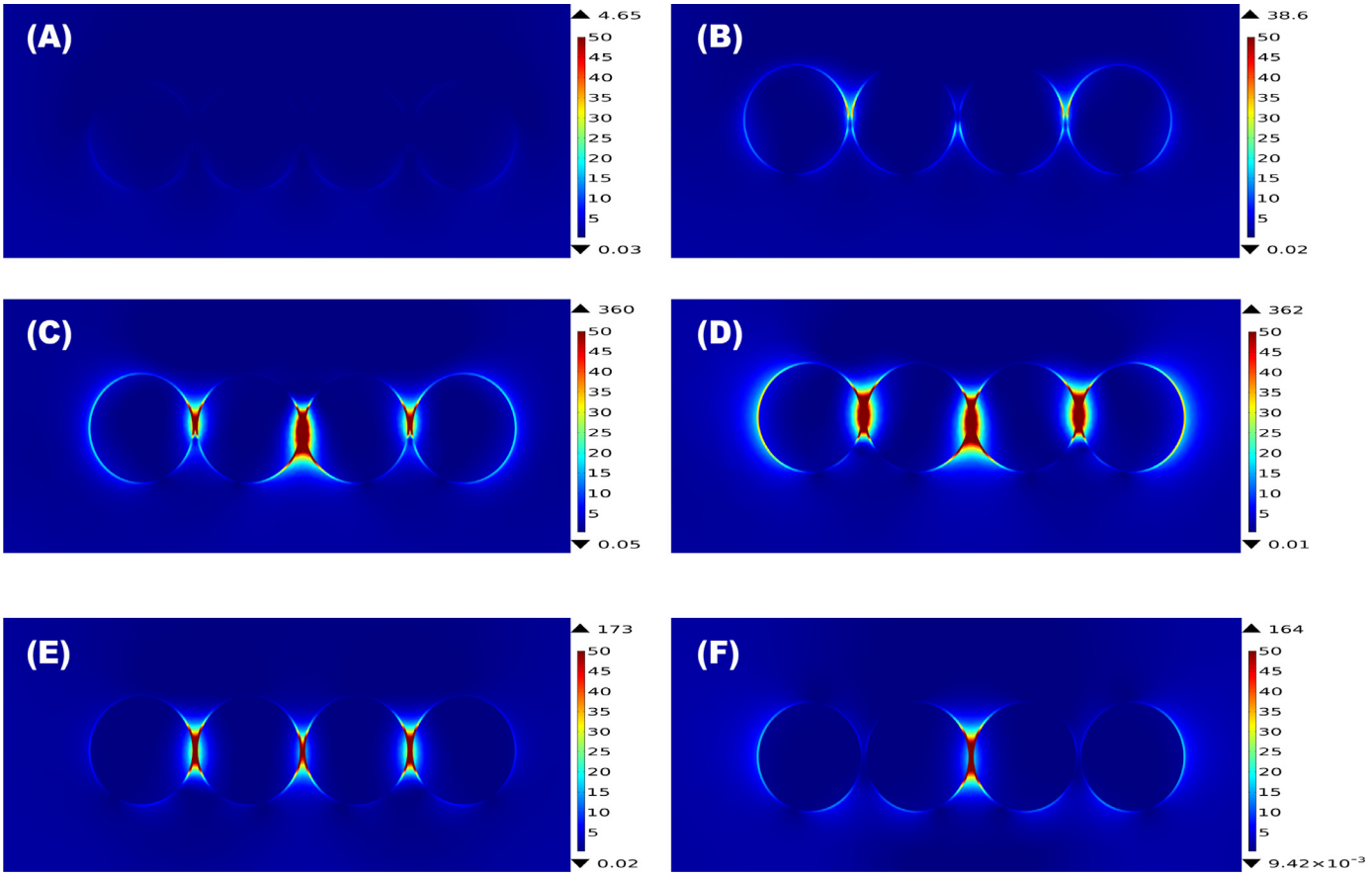

Fig. 14. Poynting vector ratio (S/S_0) for 4 particle configuration (chain) of 50 nm Au nanoparticle at $z = 0$ (symmetry plane) suspended into n=2 dielectric medium under TM polarized laser: (A) λ=532 nm (B) λ=580 nm (C) λ=620 nm (D) λ=650 nm (E) λ=700 nm (F) λ=800 nm.

dielectric medium due to the effect of confined plasmon modes. Similar to the previous case, the maximum Poynting vector ratio (S/S_0), rather than the electric field intensity ($|I/I_0|$), predicts the resonant wavelength in the dielectric medium that gives the maximum absorption cross-section. This could be due to the scattering effect that the total emission via calculation of Poynting vector provides the right approach rather than the maximum electric field intensity to predict the conditions that maximize the absorption cross-section.

Fig. 13(B) and (C) illustrates the scattering and extinction cross-section, respectively. It is observed from Fig. 13(C) that the 800 nm laser source provides the maximum extinction cross-section, which is around 2.7×10^{-13} m^2 and corresponds to extinction efficiency of 8.6 when Au nanoparticle chain is suspended into n=1.2 dielectric medium. This implies that 800 nm wavelength is most likely the resonant frequency. The local maximum is also observed similarly as in the Au nanoparticle dimer case between 620 nm when nanoparticle suspended in n=2 dielectric medium which implies the 620 nm is another resonant frequency. It is observed that 620 nm and n=2 dielectric medium is the resonant local lower peak for both Au nanoparticle dimer and in 4 particle configuration (chain) cases. This could be explained by the contribution of the dipole-dipole modes within $n = 2$ dielectric medium at lower wavelength, 620 nm. However, effect of dielectric medium is observed very important for the plasmon gap coupling due to various modes in terms of achieving the maximum extinction cross-section as well as the corresponding resonant frequency.

Fig. 13(D) also illustrates the single-scattering albedo (w). As for the Au nanoparticle dimer case, scattering is highly dominant over absorption at longer wavelengths >700 nm regardless of the dielectric medium by about 90%. Extinction is dominated by absorption at lower wavelengths, between 400 and 550 nm, regardless of the dielectric medium. Very strong near-field scattering that happens at longer wavelength; in particular at 800 nm, within a dielectric medium of n=1.2 and n=1.52 for 50 nm radius 4 particle configuration (chain) and nanoparticle dimer, respectively results in highest extinction. Thus, the effect of dielectric medium is seen as very important for obtaining the highest extinction as well as the resonant frequency.

The modes due to plasmonic coupling between the nanoparticles can be observed in different ways as illustrated in Fig. 14. Highly confined near-field electromagnetic energy which also represents the high absorption cross-section when the particles are suspended into n=2 dielectric medium can be observed from Fig. 14(D) for 650 nm and TM polarized laser irradiation. This high near-field confinement is also observed between the two adjacent nanoparticles whereas at lower and higher wavelength, the confinement between the two adjacent nanoparticles start to be different. For instance, at 580 nm wavelength which is observed from Fig. 14(B), the higher confinement happens at the outer particles near the center region. For 800 nm, the particles at the center region exhibits very strong confinement as opposed to outer particles. Thus, the behavior of collective plasmon modes are observed as strongly dependent on wavelength due to the fact that such collective optical electromagnetic enhancement spans through all particles in the chain implies higher group velocity v_g and lower homogenous linewidth Γ of the plasmon oscillations that are characterized by the wavelength change significantly.

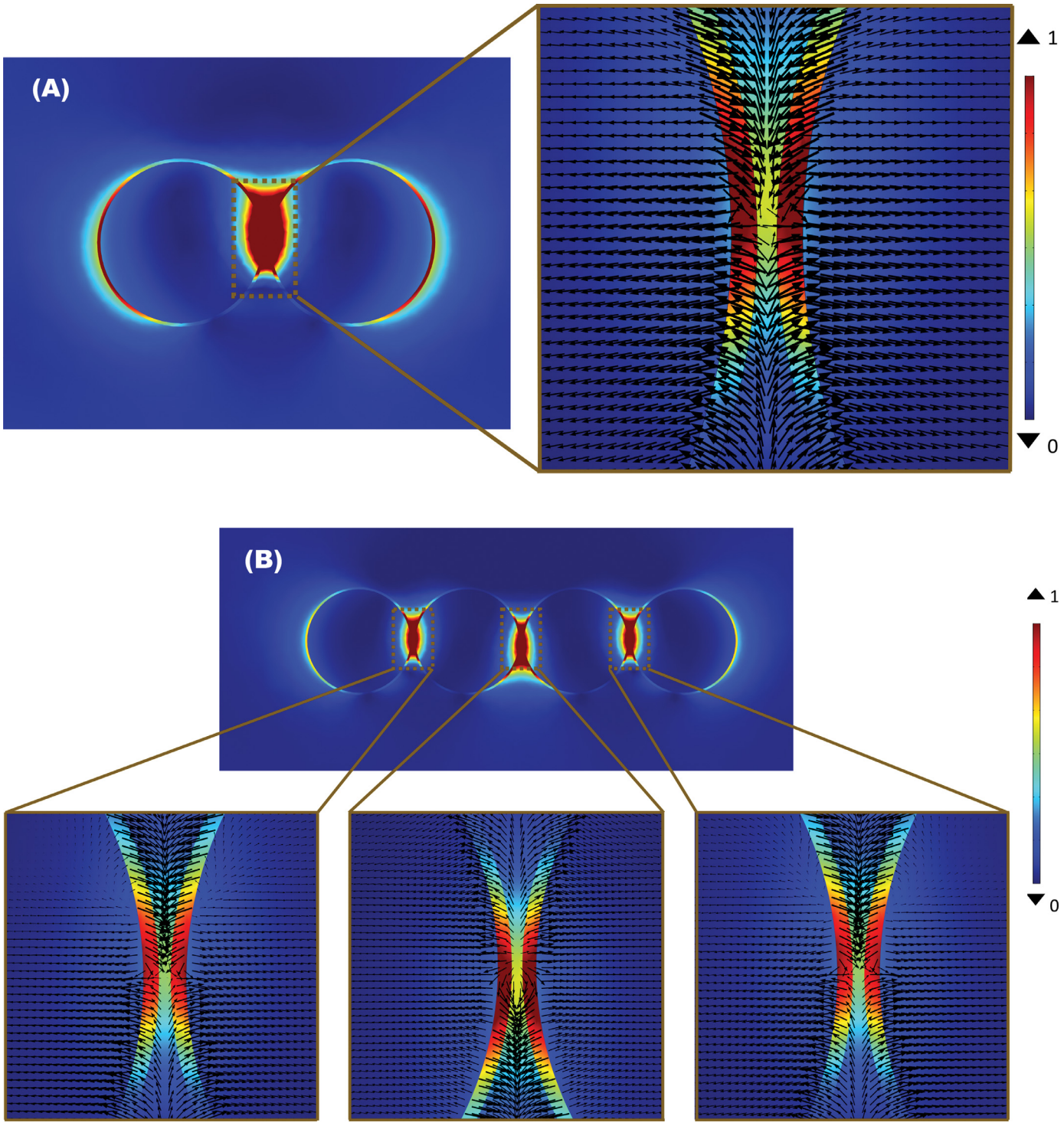

Fig. 15. Normalized Poynting vector ratio (S/S_{max}) for 50 nm (chain) of 50 nm Au nanoparticle at $z = 0$ (symmetry plane) suspended into n=2 dielectric medium under TM polarized laser: (A) Dimer Configuration, λ=620 nm (B) Chain Configuration, λ=650 nm.

3.4. Direction of poynting vector on dimer and chain configuration

When the absorption or scattering cross-section reaches to a peak point, a vortex like Poynting vector distribution is observed around the nanoparticles [47]. Similarly, such vortex type energy flow distribution is observed for 50 nm Au nanoparticle dimer (Θ=0°) and 4 particle configuration (chain) (Θ=0°) at the corresponding dielectric media and laser wavelength that results in achieving highest absorption cross-section. Fig. 15 illustrates the Poynting vector directions for 50 nm Au nanoparticle dimer at λ=620 nm and 4 particle configuration (chain) at λ=650 nm suspended into n=2 dielectric medium under TM polarized laser.

It is observed that the energy flow lines between the adjacent nanoparticle at the top is almost perpendicular to the incident illumination and at the center region, it aligns with the direction of incident wave polarization. Thus, a vortex type of flow is observed for both dimer and chain type of configuration. However, the directions of the Poynting vector in the chain configuration change depending on the position of the gap within the particle chain, as

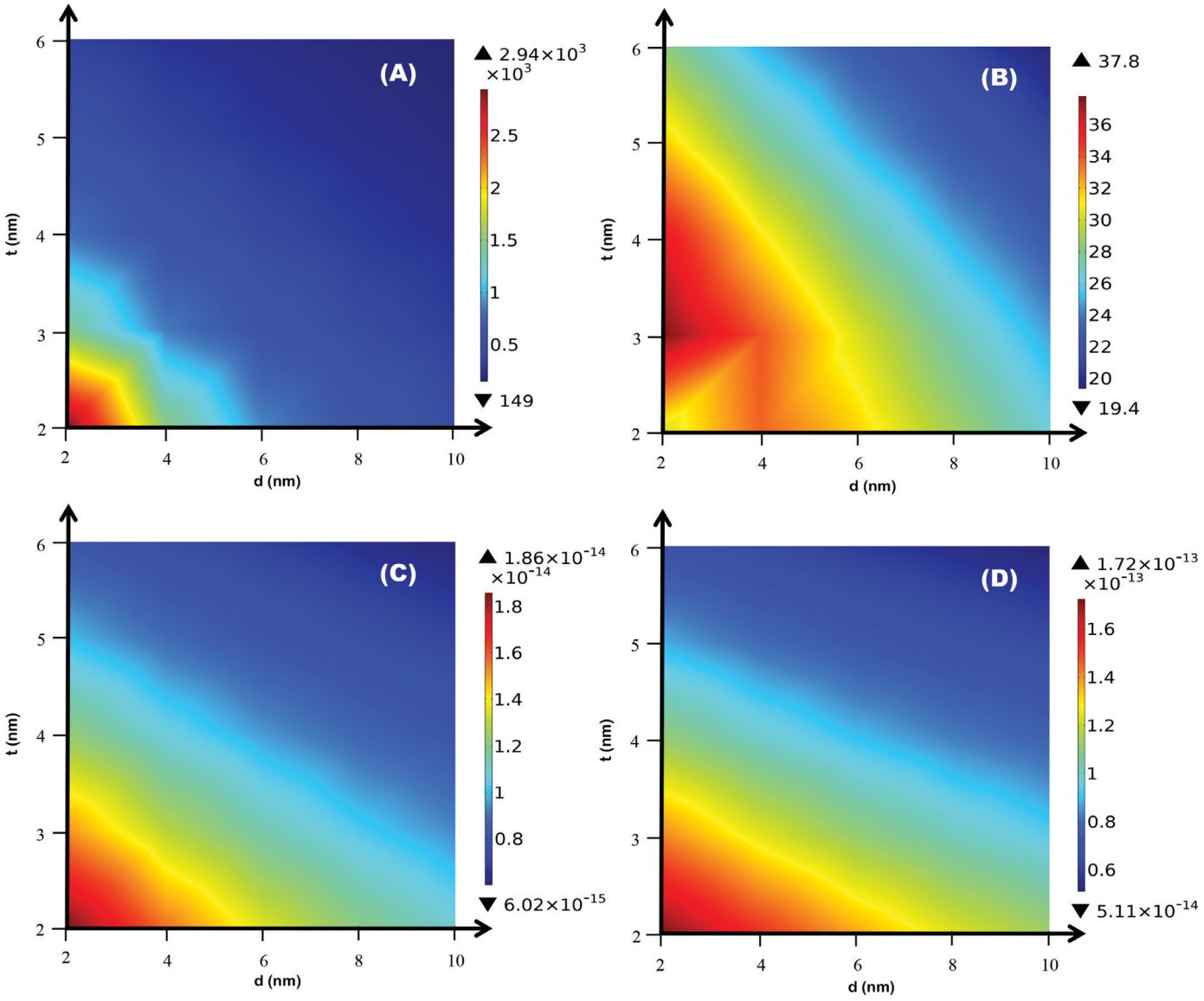

Fig. 16. 50 nm radius Au nanoparticle dimer suspended into n=1.52 dielectric medium under 800 nm TM polarized laser: (A) Maximum electric field intensity ($|I/I_0|$) distribution (B) Maximum Poynting vector ratio (S/S_0) (C) Absorption cross-section (m^2) (D) Extinction cross-section (m^2).

shown in Fig. 15, reflecting the differences in the plasmonic modes for the chain configuration compared to those for the dimer.

3.5. Effect of dielectric shell thickness and nanoparticle distance variation on particle configurations

Understanding the effect of dielectric shell thickness and nanoparticle distance variation on investigated particle configurations are important for further characterization of the near-field plasmonic coupling. Thus, dielectric shell thickness (t) and the adjacent nanoparticle distance (d) are varied from 2 to 6 nm and 2–10 nm, respectively for the scaling analysis for 50 nm Au nanoparticle dimer (Θ=0°) suspended into n=1.52 dielectric medium under 800 nm TM polarized laser, for which the highest extinction cross-section is observed within the investigated dielectric medium and the wavelength range.

It is observed from Fig. 16(A) that maximum electric field intensity dramatically decreases when t>5 nm even for small d. This implies that the dielectric shell thickness could diminish the near-field coupling for high values. The reduction of the near-field plasmonic coupling for thick shell values leads to decrease in absorption and extinction cross-section which is also observed from Fig. 16(C) and (D). However, it is interesting that increase of t from 2 nm to about 3 nm still leads to increasing the maximum Poynting vector ratio as shown in Fig. 16(B). This could be due to observed very high near-field scattering at 800 nm, TM polarized light illumination in n=1.52 dielectric media that could still have an impact on local energy flow.

Reducing the space between the particles results in monotonic temperature increase during light source irradiation as shown in earlier theoretical modeling [48]. As mentioned earlier, quantum effects which become important for d <1 nm are not taken into consideration in this work. In the quantum regime, highly nonlinear effects are observed due to electron tunneling and electric field polarization although there is more research needed on these effects [49,50]. Due to dielectric shell, dielectric medium and the agglomeration effects, it is likely expected to have at least 1 nm gap between the adjacent nanoparticles. Thus, classical regime as

assumed in this work can describe the characteristics of the near-field plasmonics of Au nanoparticles coated with nanoparticle shell and suspended into dielectric media. It is observed that precise design is very important at the nanoscale to increase the local field enhancement and coupling strength for the enhanced plasmonic behavior. Such plasmonically enhanced nanoparticle structures could be potentially desirable for many photonic applications [51,52].

4. Conclusion

Characteristics of optical electromagnetic energy propagation in Au nanoparticle dimers with nanoparticle radii of 25 nm, 50 nm, and 100 nm, and 4 nanoparticle configuration (chain) with 50 nm particle radius, surrounded with dielectric shell and suspended in different media are determined using finite-difference frequency-domain simulations. Very large increases in field intensity (up to 1500 fold) can be obtained at 25 nm radius Au nanoparticle dimer having no dielectric shell with particles having 30° relative angle to the electric field in dielectric medium (n=1.33) under λ=532 nm, TM polarized light. It is observed that using 2 nm thick dielectric shell can enhance the plasmonic behavior of the Au nanoparticles; such dielectric shells may also be beneficial in controlling oxidation and agglomeration. Dielectric medium is observed as very important for tuning the resonant wavelength. It is seen that maximum Poynting vector ratio (S/S_0) as opposed to electric field intensity ($|I/I_0|$) predicts the resonant wavelength that is achieved in the dielectric medium well, and correspondingly the wavelength that gives the maximum absorption cross-section. Very high maximum Poynting vector ratio (up to 500) can be obtained at 50 nm radius Au nanoparticle by arranging as dimer or 4 particle configuration (chain). Dimer configuration is observed to yield about 25% larger maximum Poynting vector ratio than 4 particle configuration (chain) when the nanoparticles are suspended into dielectric medium where n=2. It is observed that Au nanoparticles surrounded with dielectric shell and suspended in various media exhibit different plasmonic effects within investigated particle configurations, and also exhibit different extinction cross-section or efficiency such that extinction efficiency of 8.6 and 11.5 are observed for 4 nanoparticle configuration (chain) and nanoparticle dimer, respectively at the maximum extinction cross-section resonant conditions. Thus, the dielectric properties of the medium and dielectric shell that surrounds the Au under laser illumination become very important for near-field energy transport for further understanding of novel photonics design.

Declaration of Competing Interest

The authors declare that they have no known competing financial interests or personal relationships that could have appeared to influence the work reported in this paper.

Supplementary materials

Supplementary material associated with this article can be found, in the online version, at doi:10.1016/j.jqsrt.2020.107207.

CRediT authorship contribution statement

Anil Yuksel: Conceptualization, Methodology, Validation, Investigation, Writing - review & editing. **Michael Cullinan:** Resources. **Edward T. Yu:** Supervision, Writing - review & editing. **Jayathi Murthy:** Supervision.

References

[1] Daniel MC, Astruc D. Gold nanoparticles: assembly, supramolecular chemistry, quantum-size-related properties, and applications toward biology, catalysis, and nanotechnology. Chem Rev 2004;104(1):293–346.
[2] Kreibig U, Vollmer M. Optical properties of metal clusters, 25. Springer Science & Business Media; 2013.
[3] Amendola V, Pilot R, Frasconi M, Marago OM, Iati MA. Surface plasmon resonance in gold nanoparticles: a review. J Phys 2017;29(20):203002.
[4] Haes AJ, Zou S, Schatz GC, Van Duyne RP. A nanoscale optical biosensor: the long range distance dependence of the localized surface plasmon resonance of noble metal nanoparticles. J Phys Chem B 2004;108(1):109–16.
[5] Chong X, Abboud J, Zhang Z. Plasmonics resonance enhanced active photothermal effects of aluminum and iron nanoparticles. J Nanosci Nanotechnol 2015;15:2234–40.
[6] Ben X, Park HS. Size-dependent validity bounds on the universal plasmon ruler for metal nanostructure dimers. J Phys Chem 2012;C116:18944–51.
[7] Funston AM, Novo C, Davis TJ, Mulvaney P. Plasmon coupling of gold nanorods at short distances and in different geometries. Nano Lett 2009;9:1651–8.
[8] Jain PK, El-Sayed MA. Surface plasmon coupling and its universal size scaling in metal nanostructures of complex geometry: elongated particle pairs and nanosphere trimers. J Phys Chem 2008;C112:4954–60.
[9] Yan B, Boriskina SV, Reinhard BM. Optimizing gold nanoparticle cluster configurations (n $\leq$7) for array applications. J Phys Chem 2011;C115:4578–83.
[10] Hatef A, Meunier M. Plasma-mediated photothermal effects in ultrafast laser irradiation of gold nanoparticle dimers in water. Opt Express 2015;23(3):1967–80.
[11] Wang H. Plasmonic refractive index sensing using strongly coupled metal nanoantennas: nonlocal limitations. Sci Rep 2018;8(1):1–8.
[12] Stockman MI, Shalaev VM, Moskovits M, Botet R, George TF. Enhanced Raman scattering by fractal clusters: scale-invariant theory. Phys Rev B 1992;46(5):2821.
[13] Kneipp K, Wang Y, Kneipp H, Perelman LT, Itzkan I, Dasari RR, et al. Single molecule detection using surface-enhanced Raman scattering (SERS). Phys Rev Lett 1997;78(9):1667.
[14] Gopinath A, Boriskina SV, Premasiri WR, Ziegler L, Reinhard BM, Dal Negro L. Plasmonic nanogalaxies: multiscale aperiodic arrays for surface-enhanced Raman sensing. Nano Lett 2009;9(11):3922–9.
[15] Khlebtsov NG, Trachuk LA, Mel'nikov AG. The effect of the size, shape, and structure of metal nanoparticles on the dependence of their optical properties on the refractive index of a disperse medium. Opt Spectrosc 2005;98(1):77–83.
[16] Miller MM, Lazarides AA. Sensitivity of metal nanoparticle surface plasmon resonance to the dielectric environment. J Phys Chem B 2005;109(46):21556–65.
[17] Schuller JA, Barnard ES, Cai W, Jun YC, White JS, Brongersma ML. Plasmonics for extreme light concentration and manipulation. Nat Mater 2010;9(3):193.
[18] Hogan NJ, Urban AS, Ayala-Orozco C, Pimpinelli A, Nordlander P, Halas NJ. Nanoparticles heat through light localization. Nano Lett 2014;14(8):4640–5.
[19] Chen H, Kou X, Yang Z, Ni W, Wang J. Shape-and size-dependent refractive index sensitivity of gold nanoparticles. Langmuir 2008;24(10):5233–7.
[20] Tanabe K. Field enhancement around metal nanoparticles and nanoshells: a systematic investigation. J Phys Chem C 2008;112(40):15721–8.
[21] Khlebtsov BN, Khlebtsov NG. Biosensing potential of silica/gold nanoshells: sensitivity of plasmon resonance to the local dielectric environment. J Quant Spectrosc Radiat Transfer 2007;106(1–3):154–69.
[22] Aden AL, Kerker M. Scattering of electromagnetic waves from two concentric spheres. J Appl Phys 1951;22(10):1242–6.
[23] Yuksel A, Cullinan M. Modeling of nanoparticle agglomeration and powder bed formation in microscale selective laser sintering systems. Addit Manufact 2016;12:204–15.
[24] Yuksel A, Yu ET, Cullinan M, Murthy J. Effect of particle size distribution on near-field thermal energy transfer within the nanoparticle packings. J Photon Energy 2019;9(3):032707.
[25] Yuksel A, Yu ET, Cullinan M, Murthy J. Thermal transport in nanoparticle packings under laser irradiation. J Heat Transfer 2020;142(3).
[26] Yuksel A, Cullinan M, Murthy J. Thermal energy transport below the diffraction limit in close-packed metal nanoparticles. *ASME 2017 Heat Transfer Summer Conference* (pp. V002T13A005-V002T13A005). American Society of Mechanical Engineers; 2017.
[27] Yuksel A, Edward TY, Cullinan M, Murthy J. Uncertainty analysis of near-field thermal energy transfer within nanoparticle packing. In: 2018 17th IEEE Intersociety Conference on Thermal and Thermomechanical Phenomena in Electronic Systems (ITherm); 2018. p. 46–50. IEEE.
[28] Zhang W, Li Q, Qiu M. A plasmon ruler based on nanoscale photothermal effect. Opt Express 2013;21(1):172–81.
[29] Pal SK, Chatterjee H, Ghosh SK. Manipulating the confinement of electromagnetic field in size-specific gold nanoparticles dimers and trimers. RSC Adv 2019;9(72):42145–54.
[30] Rakić AD, Djurišić AB, Elazar JM, Majewski ML. Optical properties of metallic films for vertical-cavity optoelectronic devices. Appl Opt 1998;37(22):5271–83.
[31] Davletshin YR, Kumaradas JC. The role of morphology and coupling of gold nanoparticles in optical breakdown during picosecond pulse exposures. Beilstein J Nanotechnol 2016;7(1):869–80.

[32] König TA, Ledin PA, Kerszulis J, Mahmoud MA, El-Sayed MA, Reynolds JR, et al. Electrically tunable plasmonic behavior of nanocube–polymer nanomaterials induced by a redox-active electrochromic polymer. ACS Nano 2014;8(6):6182–92.
[33] Jain PK, Huang W, El-Sayed MA. On the universal scaling behavior of the distance decay of plasmon coupling in metal nanoparticle pairs: a plasmon ruler equation. Nano Lett. 2007;7(7):2080–8.
[34] Nordlander P, Oubre C, Prodan E, Li K, Stockman MI. Plasmon hybridization in nanoparticle dimers. Nano Lett. 2004;4(5):899–903.
[35] Zuloaga J, Prodan E, Nordlander P. Quantum description of the plasmon resonances of a nanoparticle dimer. Nano Lett. 2009;9(2):887–91.
[36] Huang Y, Ringe E, Hou M, Ma L, Zhang Z. Near-field mapping of three-dimensional surface charge poles for hybridized plasmon modes. AIP Adv 2015;5(10):107221.
[37] Prodan E, Radloff C, Halas NJ, Nordlander P. A hybridization model for the plasmon response of complex nanostructures. Science 2003;302(5644):419–22.
[38] Halas NJ, Lal S, Chang WS, Link S, Nordlander P. Plasmons in strongly coupled metallic nanostructures. Chem Rev 2011;111(6):3913–61.
[39] Harrison RK, Ben-Yakar A. Role of near-field enhancement in plasmonic laser nanoablation using gold nanorods on a silicon substrate: reply. Opt Express 2011;19(7):6179–81.
[40] Pascale M, Miano G, Tricarico R, Forestiere C. Full-wave electromagnetic modes and hybridization in nanoparticle dimers. Sci Rep 2019;9(1):1–21.
[41] Huang Y, Ma L, Hou M, Li J, Xie Z, Zhang Z. Hybridized plasmon modes and near-field enhancement of metallic nanoparticle-dimer on a mirror. Sci Rep 2016;6:30011.
[42] Maier SA, Kik PG, Atwater HA. Observation of coupled plasmon-polariton modes in Au nanoparticle chain waveguides of different lengths: estimation of waveguide loss. Appl Phys Lett 2002;81(9):1714–16.
[43] Rechberger W, Hohenau A, Leitner A, Krenn JR, Lamprecht B, Aussenegg FR. Optical properties of two interacting gold nanoparticles. Opt Commun 2003;220(1–3):137–41.
[44] Citrin DS. Coherent Excitation Transport in Metal– Nanoparticle Chains. Nano Lett. 2004;4(9):1561–5.
[45] Willingham B, Link S. Energy transport in metal nanoparticle chains via sub-radiant plasmon modes. Opt Express 2011;19(7):6450–61.
[46] Chen T, Pourmand M, Feizpour A, Cushman B, Reinhard BM. Tailoring plasmon coupling in self-assembled one-dimensional Au nanoparticle chains through simultaneous control of size and gap separation. J Phys Chem Lett 2013;4(13):2147–52.
[47] Bashevoy MV, Fedotov VA, Zheludev NI. Optical whirlpool on an absorbing metallic nanoparticle. Opt Express 2005;13(21):8372–9.
[48] Mezeme ME, Brosseau C. Engineering nanostructures with enhanced thermoplasmonic properties for biosensing and selective targeting applications. Phys Rev E 2013;87(1):012722.
[49] Cha H, Yoon JH, Yoon S. Probing quantum plasmon coupling using gold nanoparticle dimers with tunable interparticle distances down to the subnanometer range. ACS Nano 2014;8(8):8554–63.
[50] Esteban R, Borisov AG, Nordlander P, Aizpurua J. Bridging quantum and classical plasmonics with a quantum-corrected model. Nat Commun 2012;3(1):1–9.
[51] Romero I, Aizpurua J, Bryant GW, De Abajo FJG. Plasmons in nearly touching metallic nanoparticles: singular response in the limit of touching dimers. Opt Express 2006;14(21):9988–99.
[52] Atay T, Song JH, Nurmikko AV. Strongly interacting plasmon nanoparticle pairs: from dipole– dipole interaction to conductively coupled regime. Nano Lett. 2004;4(9):1627–31.